



Improving the Photo-catalytic Efficiency of TiO₂ by Incorporation of Cobalt for Removal of Micropollutants from Wastewater

Muhammad Irfan ^{a*}, Munazza Noor ^b, Sonia Abbas ^b,
Iqra Gohar ^b, Ahtasham Raza ^c and Noor Ahmad ^{d++}

^a Department of Physics, University of Okara, 3600 Punjab, Pakistan.

^b Department of Physics, GGDC N0 2 DIK, 29111, Pakistan.

^c Integrated Environment Laboratory, Lahore, Pakistan.

^d Environmental Protection Agency-Punjab EP&CCD, Government of the Punjab, Pakistan.

Authors' contributions

This work was carried out in collaboration among all authors. Author MI writing and analyzing original manuscript. Authors MN, SA, IG and HE Each author contribute in the experimental design and writing the manuscript. Author RPP carrying out measurements. All authors read and approved the final manuscript.

Article Information

Open Peer Review History:

This journal follows the Advanced Open Peer Review policy. Identity of the Reviewers, Editor(s) and additional Reviewers, peer review comments, different versions of the manuscript, comments of the editors, etc are available here:

<https://www.sdiarticle5.com/review-history/126730>

Original Research Article

Received: 05/09/2024

Accepted: 07/11/2024

Published: 12/11/2024

ABSTRACT

The research focuses on the fabrication and use of Co-doped titanium dioxide (TiO₂) nanocrystals for efficient industrial wastewater treatment, specifically improving photocatalytic destruction of methylene blue (MB). The crystal structure, including phase identification, crystalline size, texture,

⁺⁺ Deputy Director;

*Corresponding author: Email: m.irfan6570@gmail.com;

Cite as: Irfan, Muhammad, Munazza Noor, Sonia Abbas, Iqra Gohar, Ahtasham Raza, and Noor Ahmad. 2024. "Improving the Photo-Catalytic Efficiency of TiO₂ by Incorporation of Cobalt for Removal of Micropollutants from Wastewater". *Journal of Materials Science Research and Reviews* 7 (4):753-66. <https://journaljmsrr.com/index.php/JMSRR/article/view/364>.

stress, and strain, has been verified by X-ray powder diffraction (XRD). The average crystallite size of nanocrystals decreased from 65.69 nm to 32.62 nm with the incorporation of 9% Co into the TiO₂ crystal lattice. The presence of Ti-O and C=O functional groups in the FTIR spectra shows the successful doping of Co. The optical band gap reduced from 3.39 eV for undoped TiO₂ to 3.06 eV for 9 % Co-doped TiO₂, as confirmed by UV-Vis spectroscopy. The photocatalytic activity of the samples was studied utilizing the degradation of methylene blue as a model substance. Which was substantially increased from 5.86% for pure TiO₂ to 23.01% for Co-0.9%, with a rate constant of $2.17 \times 10^{-3} \text{ min}^{-1}$. This study shows that Co-doped TiO₂ is a viable substance for wastewater management, and offers an efficient and sustainable technique for degrading MB under ambient circumstances.

Keywords: Co-doped TiO₂ nanocrystals; single step sol-gel method; photo-degradation; methylene blue dye; wastewater.

1. INTRODUCTION

Metal oxide semiconductors, advanced functional materials such as two-component (alloyed), and metal-oxide nanoparticles have a significant impact on a range of applications in science and technology [1,2,3,4,5]. In recent decades, air and water pollution in urban areas produced mainly by automobiles and the chemical industry has become a serious threat to public health [6,7]. However, toxic organic compounds like pesticides, dyes, phenols, and the associated environmental hazardous pollutants are discharged into the aquatic environment through various anthropogenic inputs [8,2,9,10,11,12]. Despite their low concentration, the presence of these contaminants is still a major concern over public health and a major obstacle to water recycling due to their bio-recalcitrant and acute toxicity [13,14,15]. The method of "advanced oxidation processes" (AOPs) appears to become the focus of intense interest when the process can be driven by solar, UV, or visible light. Among AOPs, TiO₂ is generally considered to be one of the important evergreen photocatalysts due to its desirable physical and chemical properties against photochemical corrosion, efficient photocatalytic activity, high photostability, low cost, and toxicity [16,17,18,9]. Photocatalysis involves activating a catalyst material with light energy to speed up chemical reactions. When a photocatalyst is exposed to light energy, the photons excite electrons in the valence band (VB) to the conduction band (CB), resulting in electron-hole pairs. The holes left over in the VB can react with adsorbed species like water or organic compounds, whereas, the excited electrons in the CB have a greater energy and can participate in different redox processes [19,20,12,21]. Titanium dioxide (TiO₂) [22], zinc oxide (ZnO) [23], SnO₂ [24], Fe₂O₃ [25], CuO [26], Co-doped TiO₂ [27], and tungsten

trioxide (WO₃) [24] are a few metal oxide semiconductor (MOS) materials that have shown great promise as photocatalysts [28,29,24]. Among all of these MOS TiO₂ has attained great significance in AOPs due to its remarkable features, including chemical and physical stability, non-toxicity, strong oxidative power, low cost, antibacterial activity, environmental friendliness, highly solar-activated surface, etc [30,31,32,33]. TiO₂ exists in three phases, anatase, rutile, and brookite, of which anatase and rutile are known to be potentially active materials for many applications; such as in photocatalysis, water purification, solar cells, sensors, paints, etc. But the main drawback of these systems, for many of these applications, is their absorption in the UV region, which corresponds to only 3–5% of solar radiation [34,35,9]. However, the practical application of TiO₂ is limited by two main factors. Firstly, only a small portion of the solar spectrum is absorbed in the ultraviolet UV light region due to the wide band gap nature of titania (3.2 eV) for anatase and (3.0 eV of rutile), secondly, the recombination rate of photogenerated electron-hole pairs is too high to be used for organic pollutant degradation in practice. Therefore TiO₂ needs to attain photocatalytic response in a border range extending into visible light. To solve these difficulties, numerous researchers worked on titanium dioxide semiconductors utilizing different approaches to improve the photocatalytic performance of TiO₂ [36]. Toubal et al. (2017) produced Co-doped TiO₂ nanoparticles via sol-gel synthesis and measured their electrical characteristics, finding that Co-doping significantly increased TiO₂ conductivity [27]. Chanda et al (2021) used the sol-gel spin coating approach to create Co-doped TiO₂ thin films, resulting in high refractive index TiO₂ nano-films due to the integration of Co as a dopants material in the TiO₂ lattice. Cobalt was chosen as

a dopant material because, when exposed to UV light, Co-TiO₂ forms electron-hole pairs, which may subsequently combine with water molecules and oxygen in the air to create highly reactive oxygen species such as hydroxyl radicals (OH•) [37,38,39]. These radicals are powerful oxidants capable of breaking down organic pollutants and eliminating the microbiological contaminants found in wastewater. Currently, the most frequent preparation techniques include the gas phase process, hydrothermal method, sol-gel method, solvothermal method, and detonation method. Among the several synthesis processes the most prevalent is Solgel for material preparation. Sol-gel is one of the most utilized techniques; that is used mostly for creating thin films and nano powder photocatalysts. Many studies revealed that Solgel is a very simple technique, low temperature operatable, yielding a large number of products, producing homogeneous materials with small crystallite size and greater surface area which is the essential property for nanomaterials [40,20,41,42,43,44].

In the present work, we have prepared and characterized pure TiO₂ and cobalt-doped TiO₂ with 7% and 9% doping. The reduced crystallite size of the Co-doped TiO₂ nanocrystals can change the shape of TiO₂, resulting in a higher surface-to-volume ratio and a greater number of active sites. Therefore, the photodegradation of methylene blue designated that the separation efficiency of the photogenerated electron and hole pairs was mainly improved due to Co-

doping, and this led to a much greater photocatalytic activity for organic pollutant degradation. The relationship between the morphology, structure, optical properties, and photocatalytic activities of Co-doped TiO₂ nanocrystals was investigated in detail [36].

2. MATERIALS AND METHODS

Experimental details: All precursor ingredients, including titanium butoxide IV, cobalt sulfate, and aqueous HCl, were obtained from Sigma Aldrich (Germany), and ANALAR was used to prepare the undoped and Co-doped TiO₂ nanoparticles utilizing a single-step sol-gel process. No further purification of the precursor materials was carried out; utilized as it is obtained from the seller.

Preparation of Un-doped TiO₂: The precursor Substance 10 mL of titanium butoxide (TBO) was added to with 20 mL of distilled water. After 20 minutes of constantly stirring at ambient temperature (27 °C), 5 mL concentrated HCl was added dropwise to the solution, and steering was discontinued after 40 minutes. To make xerogel, the warmed samples were dried in an oven at 150 °C for 12 hours. Bulk crystals then formed, indicating that the gel had entirely dried. The dried gel is crushed and pestled into fine powder. Calcination at 500 °C for 4 hours was performed to eliminate any probable contaminants that degrade at high temperatures from the sample.

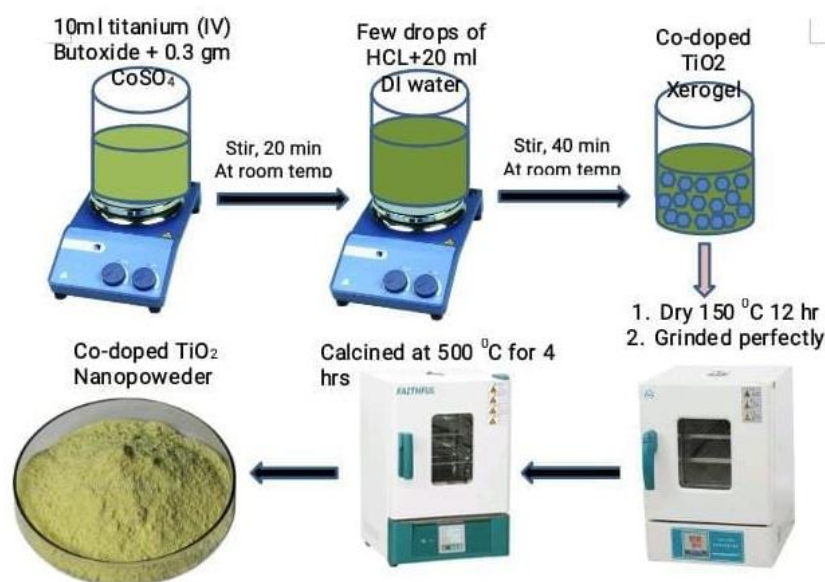


Fig. 1. Schematic diagram of Single Step Sol-gel Synthesis of Co-doped TiO₂

Preparation of Co-doped TiO₂ nanocrystals:

Titanium butoxide (TBO) 10 mL was added to (0.7 g) Co(SO₄), and after 20 minutes of constantly stirring at room temperature (27 °C), 20 mL filtered water and several drops of HCl were progressively put into the solution, and steering was stopped after 40 minutes. Warm samples were dried for 12 hours in a hot oven at 150 °C to produce xerogel. Due to the elimination of water, the dispersed gel shrank and became a viscous paste. Bulk crystals then formed, indicating that the gel was entirely dried. The dried gel was then ground into a fine powder with a mortar and pestle. To remove any suspicious impurities, Co-doped TiO₂ was calcined at 500 °C for 4 hours.

Photodegradation Activity of all prepared samples:

The resulting nanocrystals were then exposed to direct sunshine, and the photodegradation rate using methylene blue (MB) at an initial dye amount of 10 mg per 500 ml was calculated for 1 mg of catalysts per 100 ml of dye mixture. To assess the samples' photocatalytic capability, the UV-vis absorption spectra were examined by exposing them to different periods of visible light. The available sunshine exposure period ranged from 0 to 120 minutes, with 15-minute intervals.

3. RESULTS AND DISCUSSION

XRD analysis: Fig. 2 shows the XRD spectra of all the synthesized samples. The highly intense and sharp peak round of about 25° observed in all samples confirms the highly crystalline anatase phase of TiO₂ nanocrystal. The sharp crystalline peaks were observed at 2 theta degrees 25°, 38°, 48°, 55°, 56°, and 63° respectively with respective (hkl) reflection planes (101), (004), (222), (200), (105) and (112). Furthermore, Co-doped TiO₂ samples reveal mixed phases of TiO₂ anatase as well as the rutile phase. It may be due to the incorporation of Co⁺² ions can replace the Ti⁺⁴ ions in the TiO₂ lattice which can create crystal defects owing to changes in their ionic radii and valence states. This deformation in the TiO₂ crystal can alter the crystal structure, resulting in the simultaneous existence of anatase and rutile phases [45]. An extra peak observed at 42.31° in Co-doped TiO₂ samples is due to Cobalt doping can change the phase stability of TiO₂, facilitating the transition from anatase to rutile.

Co ions can reduce the energy barrier for this phase transition, resulting in the creation of an extra peak of the rutile phase. Scherrer equation (1) was used to determine the average crystallite size of all the samples.

$$D_{ave} = (0.94)\lambda / \beta \cos\theta \quad (1)$$

Here θ is the diffraction angles, D is the average crystal size, λ is the corresponding incident wavelength of the diffraction X-ray exposure (1.5418 Å), and β is the full-width half maximum (FWHM) of the diffracted peaks. The average crystallite sizes (D) for pure and Co-doped (7% and 9%) TiO₂ nano-crystals were estimated as 34.52 nm, 32.62 nm, and 65.69 nm employing equation (1), which is also presented in Table 1. The inclusion of Co⁺² ions into the TiO₂ lattice resulted in a consistent drop in the crystallite size of the TiO₂ nanocrystals. Several other essential crystal characteristics, including microstrain, dislocation density, and crystallinity, have been measured and illustrated in Table 1 [46].

FTIR Analysis: Fourier Transform Infrared (FTIR) Spectra are commonly employed to explore the structure or functional group of a multi-component system [46]. In FTIR, the intensity of IR radiation correlates to the energy gaps across quantized vibrating modes. When the infrared ray meets the energy requisite for a molecular transition, the molecule absorbs it, causing the associated vibrating mode to be stimulated. Each absorbing wavelength can be observed as a peak in the FTIR spectrum. These peaks' positions correlate to the vibrational frequencies of distinct bonds, making it possible to identify particular functional groups. The FTIR spectra of all synthesized samples pure and cobalt-doped TiO₂ NC's were observed in the wave number range of (4000 - 4000) cm⁻¹ as shown in Fig. 3. Ti-O-Ti bonds are responsible for the sharp band observed in all samples about 421 cm⁻¹. The broadband is caused by the dipole moment of nanocrystals around 1586 cm⁻¹ indicating the hydroxyl group of O-H stretching vibrations [36]. The peak at 2371 cm⁻¹ represents the asymmetric vibration (C=O) of CO₂ absorbed from the air during the thermal treatment of titanium oxides [47]. The broad bands at 1759 cm⁻¹ and 3804 cm⁻¹ are attributed to stretching and bending vibrations of water molecules (H₂O) that are adsorbed at the surface of the nanocrystals [48].

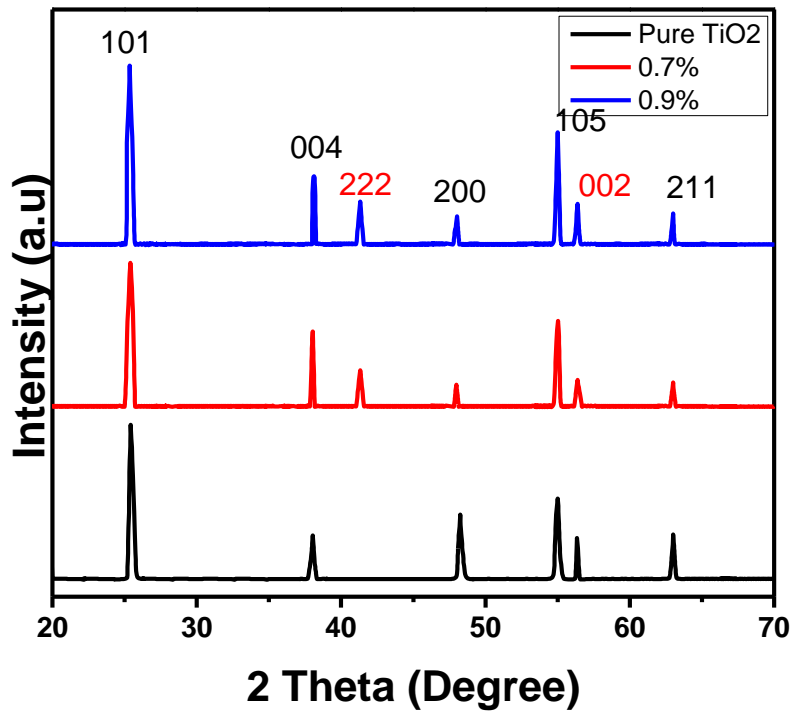


Fig. 2. XRD spectra of the pure and co-doped TiO₂ nanocrystals

Table 1. Detailed photochemical properties of pure and Co-doped TiO₂ nanocrystals

Dopants Concentration W%	Crystallize sizes (nm)	Micro strain (10^{-3})	Dislocation Density ($(\text{nm})^{-2} \times 10$)	Crystallinity %	E _g (eV)
TiO ₂ - Pure	65.69	0.584	0.8303	33.522	3.39
TiO ₂ -Co 0.7 w%	34.52	0.492	1.5909	91.164	3.27
TiO ₂ -Co 0.9 w%	32.62	0.415	1.544	55.53	3.06

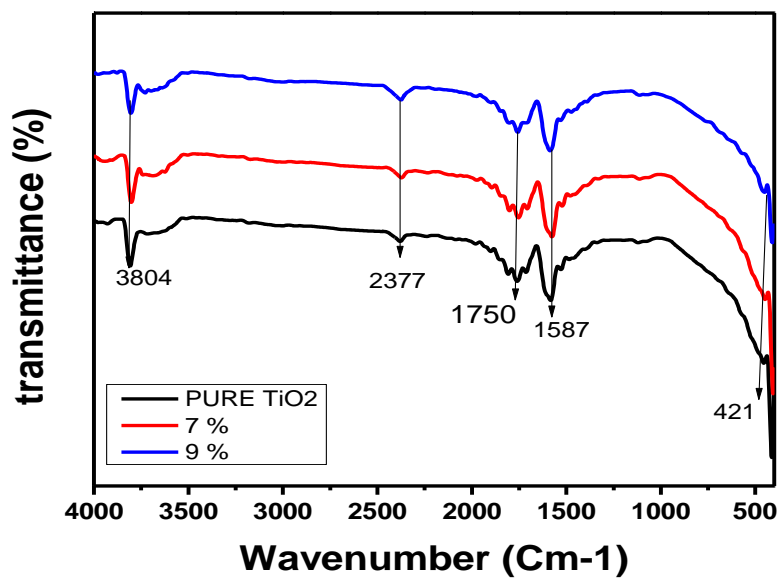


Fig. 3. FTIR spectra of the pure and co-doped TiO₂ nanocrystals

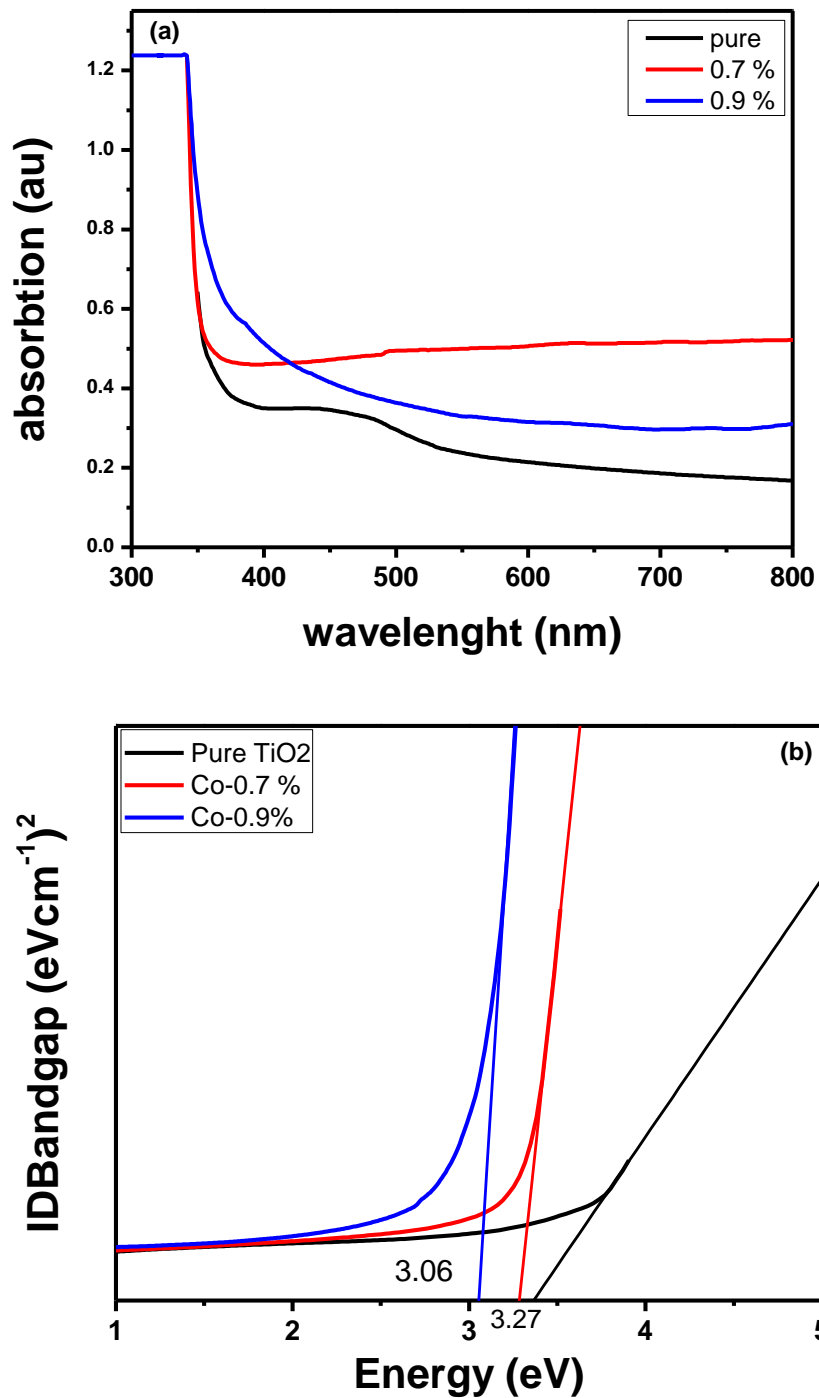


Fig. 4. (a) UV visible absorbance spectra and (b) Indirect Bandgap Vs energy (eV) of the fabricated pure, 0.7 and 0.9 % Co-doped TiO_2 nanocrystals

UV analysis: Fig. 4 depicts the UV-Vis absorbance spectra of all the produced samples, both pure and Co-doped TiO_2 , in the 200-800 nm region. Absorption peaks represent transitions between electrical energy levels. The absorption edges of pure and different concentrations of Co-

doped TiO_2 (0.7% and 9%) have been observed at 366, 379, and 405 nm, correspondingly. Fig. 4 demonstrates that the absorption edge shifts towards longer wavelengths region while the percentage of Co enhances in the TiO_2 lattice structure indicating an alternate decline in the

optical band gap of the TiO₂. The indirect band gap transition was estimated using Equation 2.

$$(\alpha h\nu)^n = A(h\nu - E_g) \quad (2)$$

In the above equation, α is the absorption coefficient calculated from UV data, h is the planks constant, $n = 2$ for the indirect allowed transition and A represents the absorbance of the material. The indirect optical band gap calculated values are 3.39 eV for pure TiO₂, 3.27 eV, and 3.06 eV for pure and 7% and 9% Co-doped TiO₂ samples [39]. The declining behavior in optical band gap E_g is caused by the addition of Co⁺² ions in TiO₂, which activates the nanocrystal material in the higher wavelength portion of the visible spectrum of light. It may be due to the development of new energy levels between the valance and conduction band of the TiO₂ crystals caused by the inclusion of Co⁺² ions. Co-doped TiO₂ has a narrower band gap due to added energy levels from dopants. These intermediate states enable electrons to switch with less energetic photons, transforming absorption to the visible spectrum and increasing the material's photocatalytic effectiveness under sunlight.

Photocatalytic activity: The produced nanocrystals were then exposed to direct sunshine, and the rate of photo-degradation using methylene blue (MB) at initial dye concentrations of 10 mg per 500 mL was calculated for 1 mg of catalysts per 100 mL of dye solution. To assess the samples' photocatalytic capacity, the UV-Vis absorption spectra were examined by exposing them to different periods of visible light. The available sunshine exposure period ranged from 0 to 120 minutes, with 15-minute intervals. A series of preliminary experiments were conducted to determine the influence of photocatalysis and adsorption on photocatalytic transformation. Photocatalysis studies were conducted at pH = 6 and a concentration of 1mg Co-doped TiO₂ in 100 ml of MB solution [49]. It is observed that the methylene blue steadily degrades over time after each 15-minute interval under continuous exposure to sunlight. Fig. 5 displays the findings of the photocatalytic decomposition of MB under visible sunlight in the presence of pure and Co-doped TiO₂ nanocrystals. Fig. (5-a) reveals very minor degradation of MB (5.86%) in the presence of

pure TiO₂ nanocrystals during 120 min exposure to direct sunlight. The degradation of MB increases significantly up to 14.76 % and 23,01 % in the presence of 0.7 and 0.9 % Co-doped TiO₂ nanocrystals. Enhancing photodegradation of MB in the presence of Co-doped TiO₂ nanocrystals owing to Photocatalyst activity is determined by two primary factors: greater surface area and increased light absorption capacity in the visible spectrum [50]. Broad humps might suggest an appearance of intermediate energy states within the band gap, which are caused by Co⁺² ions. These states, also known as "trap states" or "mid-gap states," facilitate more light absorption at lower energies than the pure band gap, which extends absorption into the visible domain of light. The photodegradation efficiency of all produced nanocrystals was determined using the following equation:

$$\text{Photodegraded efficiency \%} = (C_0 - C_t / C_0) \times 100\% \quad (3)$$

Where C_0 and C_t are before illumination and after MB degradation concentrations, respectively [51].

To further figure out how MB dye degrades photocatalytically, Fig. 6 (a,b) displays the pseudo first-order model reaction kinetics of pure and, Co-doped TiO₂. The dynamics of the first-order model are defined in Formula (4) below.

$$\ln C_0 / C_t = kt \quad (4)$$

Where C_0 and C_t represent the amount of MB degraded in exposure to direct sunlight for a total of 120 minutes, divided into 15-minute intervals. The symbols t and k represent the reaction's time and rate constants, respectively. A tauc plot was used to analyze the linear fitting vs. irradiation time of MB photocatalytic degradation, as shown in Fig. 6 (b). The projected kinetic degradation rate constant (k) can be determined by studying the gradient of the fitting curve. Under direct sunlight, it was discovered that the estimated values of (k) for pure TiO₂ and (0.7 & 0.9) % Co-doped TiO₂ are (0.45, 1.38, and 2.17) $\times 10^{-3} \text{ min}^{-1}$, as shown in Table 2. As shown in Fig. (6-b) the rate constant for MB degradation increases with an increase in the concentration of the Co in TiO₂ nanocrystals and the half-life decreases correspondingly [52].

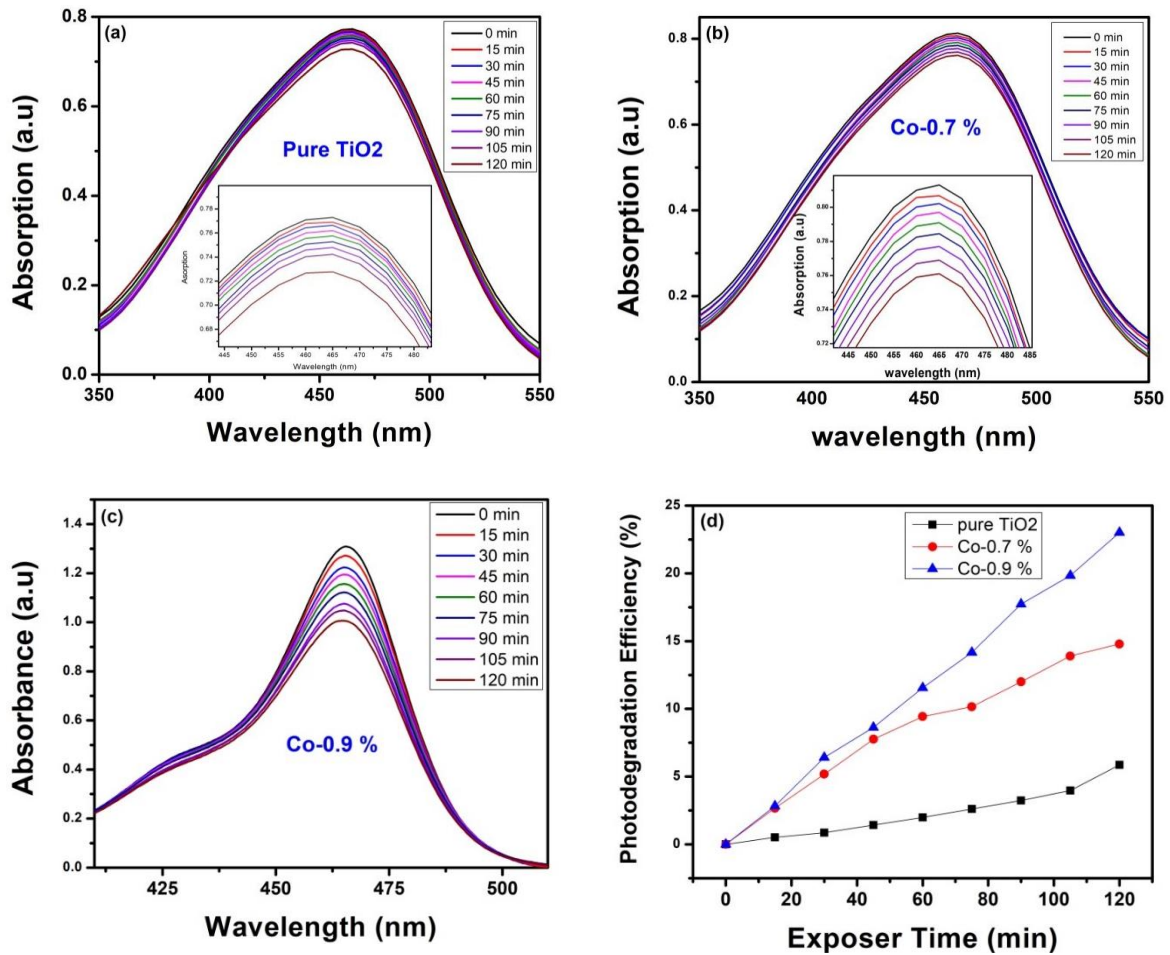


Fig. 5. UV vis absorbance (a) Pure s (b) Co-0.7 % (c) Co-0.9 % (d) Photodegradation Efficiency Vs Exposer Time of all the fabricated samples

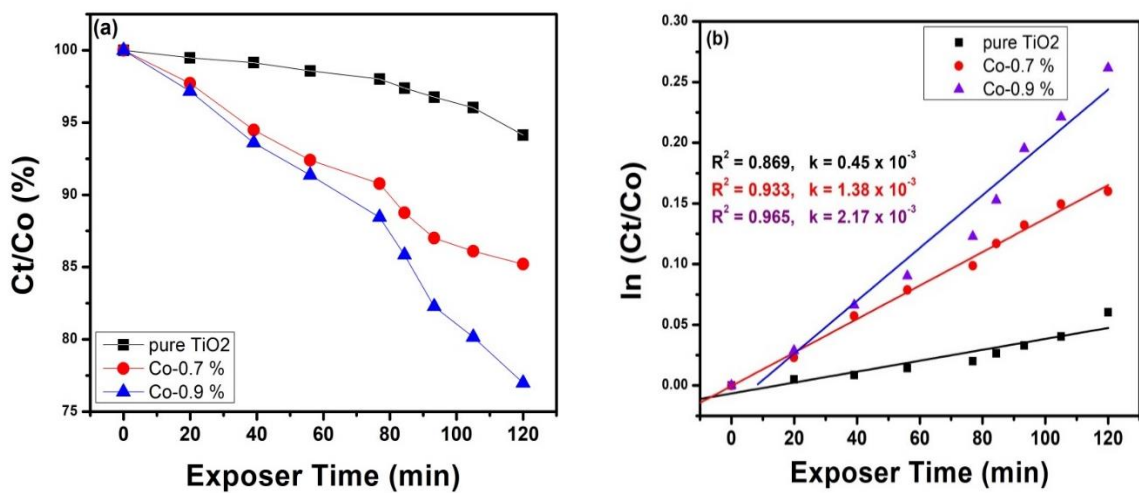


Fig. 6. Pseudo First-order model reaction kinetics (a) C_t/C₀ %, (b) ln(C_t/C₀) pure, 0.7 % and 0.9 % Co-doped TiO₂ nano-photocatalysts

Table 2. Detailed photodegradation parameters of pure and Co-doped TiO₂ added MB

Dopant Concentration w%	Rate Constant k x 10 ⁻³ (min ⁻¹)	Residual Concentration (R ²)	Half-life of Dye t _{1/2} x 10 ⁻³ (min)
Pure TiO ₂	0.45	0.869	1.54
0.7 % Co-TiO ₂	1.38	0.933	0.50
0.9 % Co-TiO ₂	2.17	0.965	0.32

Photo-degradation mechanism: When the MB solution is in the presence of fabricated nanocrystals subjected to direct sunlight, Co-doped TiO₂ absorbs photons with energy equivalent to or exceeding its band gap. This energy stimulates electrons from the valence band (VB) to the conduction band (CB), resulting in electron-hole pairs (e⁻, h⁺). Photogenerated electrons migrate to the outermost layer of TiO₂ nanocrystals and transform molecular oxygen (O₂) into reactive superoxide (O₂⁻). After holes created by sunlight approach the surface, they can oxidize hydroxide ions (OH⁻) or water (H₂O), producing hydroxyl radicals (•OH). Methylene blue molecules get destroyed by hydroxyl radicals (•OH) and superoxide radicals (O₂⁻), causing the complicated chemical arrangement of MB to disintegrate into smaller, harmless, or environment-friendly substances like CO₂, H₂O, and other least hazardous inorganic elements.

Cobalt ions (Co⁺²) provide energy levels to the band gap of TiO₂. This lowers the band gap energy, allowing visible light to be absorbed while also improving electron-hole pair separation by capturing electrons or holes, lowering their recombination rate. Photogenerated electrons in the CB and holes in the VB undergo redox interactions with water (H₂O) and oxygen (O₂) molecules adsorbed on the TiO₂ surface. These processes produce reactive oxygen species (ROS), such as hydroxyl radicals (•OH) and superoxide anions (O₂⁻).

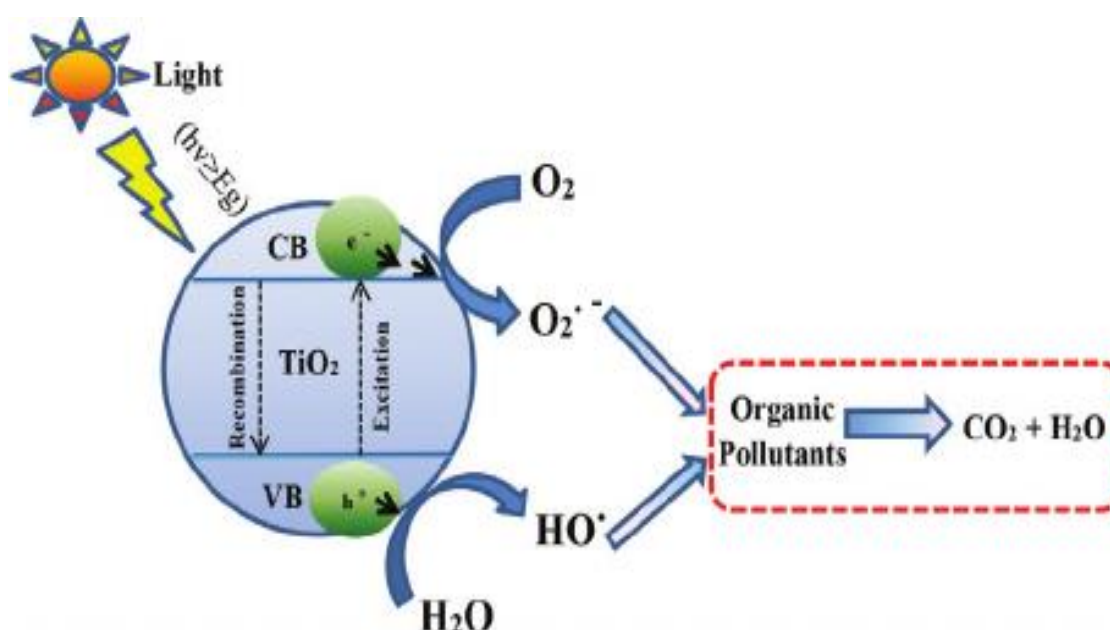
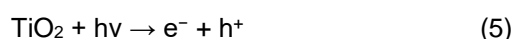
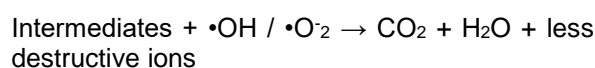
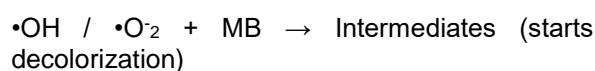
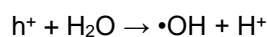
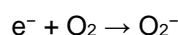
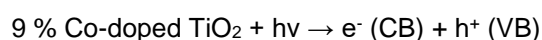
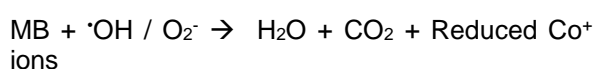


Fig. 7. Schematic diagram of the photo-degradation of MB in the presence of Co-doped TiO₂ nanocrystals

Table 3. Comparison of current research with previous similar studies

Commercial Dye	Photocatalyst	Quantity	Degradation %	Exposer Time (min)	Reference
RB19	ZnO-KIL 2-1	800 mg/L	22	120	[53]
MB	Cu-TiO ₂	5 mg/L	17	120	[54]
MG	Cd-ZnO	500 mg/L	18	120	[55]
SMX	Co-Doped TiO ₂	1.65 mg/L	9.88	120	[56]
MB	Co-TiO ₂	1 mg/L	23.01	120	Current study

The ROS produced in the earlier phase are highly reactive and can oxidize organic pollutants in MB dye, reducing them to smaller, less hazardous molecules like water and carbon dioxide.



Doping TiO₂ with cobalt results in a change in TiO₂'s electronic arrangement. It is useful for aiding in the appropriate separation of electron-hole pairs and shifting light absorption to the visible range, hence boosting photocatalytic activity under sunlight. The use of a Co-doped TiO₂ catalyst for photocatalytic degradation is extremely effective and can be reused multiple times without losing effectiveness. This makes it a sustainable solution for treating dye-contaminated water.

Table 3 presents a comparison of the current study to similar efforts in the literature. The current study outperforms several earlier publications.

4. CONCLUSION

A single-step Sol-gel synthesis technique was used to successfully produce Co-doped TiO₂ nanocrystals, which were then used to degrade MB, a commercial dye widely used in the cotton and paint industries. The synthesized nanocrystals were characterized through various material characterization techniques such as XRD, FTIR, and UV which confirm the successful doping of Cobalt into TiO₂ lattice with enhanced photocatalytic and optical properties. The increase in the Cobalt concentration in the TiO₂ crystal lattice reveals a gradual increase in the photodegradation of MB and also results in the reduction of the band gap energies of the TiO₂ nanocrystals. Overall Co-doped TiO₂ has stronger photocatalytic activity than pure TiO₂

due to improved light absorption, charge separation, ROS production, stability, and reusability. Future research should focus on developing better synthesis methods to control the size, shape, and dispersion of Co-doped TiO₂ nanocrystals, resulting in improved photocatalytic capabilities.

DISCLAIMER (ARTIFICIAL INTELLIGENCE)

Author(s) hereby declare that NO generative AI technologies such as Large Language Models (ChatGPT, COPILOT, etc.) and text-to-image generators have been used during the writing or editing of this manuscript.

DATA AVAILABILITY STATEMENT

The datasets generated and analyzed during the current study are available from the corresponding author upon reasonable request.

ACKNOWLEDGEMENT

The authors extend their appreciation to the Deanship of Research and Graduate Studies at King Khalid University, Saudi Arabia for funding this work through the Large Groups Project under grant number R.G.P2/175/45 and also thankful to the Deanship of Graduate Studies and Scientific Research at University of Bisha for supporting this work through the Fast-Track Research Support Program.

COMPETING INTERESTS

Authors have declared that no competing interests exist.

REFERENCES

1. Irfan M et al. Improving photocatalytic efficiency of ZnO nanoflowers through gold

- incorporation for Rhodamine B photodegradation. *Opt Mater (Amst)*. 2024, Aug;154:115681.
DOI: 10.1016/j.optmat.2024.115681.
2. Chavali MS, Nikolova MP. Metal oxide nanoparticles and their applications in nanotechnology. *SN Appl Sci*. 2019, Jun 1;1(6):592-3.
DOI: 10.1007/s42452-019-0592-3.
 3. Maragatha J, Rajendran S, Endo T, Karuppuchamy S. Microwave synthesis of metal doped TiO₂ for photocatalytic applications. *J Mater Sci Mater Electron*. 2017, Apr;28(7):5281-7.
DOI: 10.1007/s10854-016-6185-7.
 4. Deng Y. Sensing mechanism and evaluation criteria of semiconducting metal oxides gas sensors. In: *Semiconducting Metal Oxides for Gas Sensing*. Singapore: Springer. 2019;23-51. DOI: 10.1007/978-981-13-5853-1_2.
 5. Krishna KG, Parne S, Pothukanuri N, Kathirvelu V, Gandhi S, Joshi D. Nanostructured metal oxide semiconductor-based gas sensors: A comprehensive review. *Sensors Actuators A Phys*. 2022, Jul;341:113578.
DOI: 10.1016/j.sna.2022.113578.
 6. Aqeel M, Ikram M, Imran M, Ul-hamid A. TiO₂ Co-doped with Zr and Ag shows highly suitable for treatment of polluted water. *RSC Adv*. 2020;2:42235-48.
DOI: 10.1039/d0ra08718a.
 7. Zhao Y et al. Rapid proton exchange between surface bridging hydroxyls and adsorbed molecules on TiO₂. *Appl Catal B Environ*. 2020;277:119234.
DOI: 10.1016/j.apcatb.2020.119234.
 8. Kononov A, et al. Online breath analysis using metal oxide semiconductor sensors (electronic nose) for diagnosis of lung cancer. *J Breath Res*. 2020;14(1):1-10.
DOI: 10.1088/1752-7163/ab433d.
 9. Navidpour AH, Abbasi S, Li D, Mojiri A, Zhou JL. Investigation of advanced oxidation process in the presence of TiO₂ semiconductor as photocatalyst: Property, principle, kinetic analysis, and photocatalytic activity. *Catalysts*. 2023 Jan;13(2):232.
DOI: 10.3390/catal13020232.
 10. Soni V, Singh AN, Singh P, Gupta A. Photocatalytic dye-degradation activity of nano-crystalline Ti_{1-x}M_xO_{2-δ} (M = Ag, Pd, Fe, Ni and x = 0, 0.01) for water pollution abatement. *RSC Adv*. 2022; 12(29):18794-805.
DOI: 10.1039/d2ra02847f.
 11. Mohammed R, Ali MEM, Gomaa E, Mohsen M. Green ZnO nanorod material for dye degradation and detoxification of pharmaceutical wastes in water. *J Environ Chem Eng*. 2020;8(5): 104295.
DOI: 10.1016/j.jece.2020.104295.
 12. Verma N, et al. Characterization of Fabricated Gold-Doped ZnO Nanospheres and Their Use as a Photocatalyst in the Degradation of DR-31 Dye. *J Nanomater*. 2022;2022:7532332.
DOI: 10.1155/2022/7532332.
 13. Irfan M, Khan MI, Al Huwayz M, Alwadai N. Synthesis, characterization, and photodegradation assessment of Ni and Cd-doped TiO₂ nanocrystals via sol-gel method for methylene blue under sunlight. *Dig J Nanomater Biostruct*. 2024;19(2): 953-66.
DOI: 10.15251/DJNB.2024.192.953.
 14. Jo WK, Kim YG, Tonda S. Hierarchical flower-like NiAl-layered double hydroxide microspheres encapsulated with black Cu-doped TiO₂ nanoparticles: Highly efficient visible-light-driven composite photocatalysts for environmental remediation. *J Hazard Mater*. 2018 Sep; 357:19-29.
DOI: 10.1016/j.jhazmat.2018.05.038.
 15. Samadi A, et al. Stratum corneum hydration in healthy adult humans according to the skin area, age and sex: A systematic review and meta-analysis. *J Eur Acad Dermatol Venereol*. 2022, Oct;36(10):1713-21.
DOI: 10.1111/jdv.18297.
 16. Yang Z, Qin L, Tian P, Zhang Y. Review of N and metal co-doped TiO₂ for water purification under visible light irradiation 2. Principle of Photocatalytic Oxidation Process. *IPCBEE*. 2014;78:31-40.
DOI: 10.7763/IPCBEE.
 17. Chen Y, Zeng D, Zhang K, Lu A, Wang L, Peng DL. Au-ZnO hybrid nanoflowers, nanomultipods and nanopyramids: One-pot reaction synthesis and photocatalytic properties. *Nanoscale*. 2014;6(2):874-81.
DOI: 10.1039/C3NR04558G.
 18. Juárez-Cortazar DE, et al. Doping of TiO₂ using metal waste (Door Key) to improve its photocatalytic efficiency in the mineralization of an emerging contaminant

- in an aqueous environment. *Water*. 2022, Apr;14(9):1389.
DOI: 10.3390/w14091389.
19. Challagulla S, Tarafder K, Ganesan R, Roy S. Structure sensitive photocatalytic reduction of nitroarenes over TiO₂. *Sci Rep*. 2017, Aug;7(1):8783.
DOI: 10.1038/s41598-017-08599-2.
 20. Khlyustova A, et al. Doped TiO₂: The effect of doping elements on photocatalytic activity. *Mater Adv*. 2020;1(5):1193-1201.
DOI: 10.1039/d0ma00171f.
 21. Lee SF, Jimenez-Relinque E, Martinez I, Castellote M. Effects of mott-schottky frequency selection and other controlling factors on flat-band potential and band-edge position determination of TiO₂. *Catalysts*. 2023, Jun;13(6):1000.
DOI: 10.3390/catal13061000.
 22. Tomić J, Malinović N. Titanium dioxide photocatalyst: Present situation and future approaches. *AIDASCO Rev*. 2023, Jun;1(2):26-30.
DOI: 10.59783/aire.2023.27.
 23. Modi S, et al. Photocatalytic degradation of methylene blue dye from wastewater by using doped zinc oxide nanoparticles. *Water*. 2023, Jun;15(12):2275.
DOI: 10.3390/w15122275.
 24. Li Q, Zeng W, Li Y. Metal oxide gas sensors for detecting NO₂ in industrial exhaust gas: Recent developments. *Sensors Actuators B Chem*. 2022, May 15;359:131579.
DOI: 10.1016/j.snb.2022.131579.
 25. Al-Musawi TJ, et al. Degradation of amoxicillin under a UV or visible light photocatalytic treatment process using Fe₂O₃/bentonite/TiO₂: Performance, kinetic, degradation pathway, energy consumption, and toxicology studies. *Optik (Stuttg)*. 2023, Feb;272:170230.
DOI: 10.1016/j.ijleo.2022.170230.
 26. Ullah F, Ghani U, Mohamed Saheed MS. A PN-type CuO@TiO₂ nanorods heterojunction for efficient PEC water splitting: DFT model and experimental investigation on the effect of calcination temperature. *Int J Hydrogen Energy*; 2023, Aug.
DOI: 10.1016/j.ijhydene.2023.07.159.
 27. Toubal B, Bensaha R, Yakuphanoglu F. The influence of copper-cobalt co-doping on optical and electrical properties of nanostructures TiO₂ thin films prepared by sol-gel. *J Sol-Gel Sci Technol*. 2017; 82(2):478-89.
DOI: 10.1007/s10971-017-4337-8.
 28. Hasanah AU, Gareso PL, Rauf N, Tahir D. Photocatalytic performance of zinc oxide and metal-doped zinc oxide for various organic pollutants. *Chem Bio Eng Rev*. 2023;10(5):698-710.
DOI:10.1002/cben.202300004.
 29. Gao X, Zhang T. An overview: Facet-dependent metal oxide semiconductor gas sensors. *Sensors Actuators B Chem*. 2018;277:604-633.
DOI:10.1016/j.snb.2018.08.129.
 30. Patricia M, Vega B, Aracely MH, Luis HJ, Mar G, Hinojosa-Reyes VRL. Visible light photocatalytic activity of sol-gel Ni-doped TiO₂ on p-arsanilic acid degradation. *J Sol-Gel Sci Technol*; 2018.
DOI:10.1007/s10971-018-4579-0.
 31. Trzeciak M, Miądlicki P, Tryba B. Enhanced degradation of ethylene in thermo-photocatalytic process using TiO₂/nickel foam: Reaction mechanism; 2023.
DOI:10.20944/preprints202311.1352.v1.
 32. Chambers C, Stewart SB, Su B, Jenkinson HF, Sandy JR, Ireland AJ. Silver doped titanium dioxide nanoparticles as antimicrobial additives to dental polymers. *Dent Mater*. 2017;33(3).
DOI:10.1016/j.dental.2016.11.008.
 33. Bahadur J, Agrawal S, Parveen A, Jawad A, Ashraf SSZ, Ghalib RM. Micro-structural, optical and dielectric properties of Ag doped TiO₂ synthesized by sol-gel method. *Mater Focus*. 2015;4(2):134-141.
DOI:10.1166/mat.2015.1228.
 34. Choudhury B, Choudhury A. Luminescence characteristics of cobalt doped TiO₂ nanoparticles. *J Lumin*. 2012; 132:178-184.
DOI:10.1016/j.jlumin.2011.08.020.
 35. Nigussie GY et al. Antibacterial activity of Ag-doped TiO₂ and Ag-doped ZnO nanoparticles. *Int J Photoenergy*. 2018; 2018:5927485.
DOI:10.1155/2018/5927485.
 36. Singaram B, Jeyaram J, Rajendran R, Arumugam P. Visible light photocatalytic activity of tungsten and fluorine codoped TiO₂ nanoparticle for an efficient dye degradation; 2018.
 37. Anju KR, Thankapan R, Rajabathar JR, Al-Lohedan HA. Hydrothermal synthesis of nanosized (Fe, Co, Ni)-TiO₂ for enhanced

- visible light photosensitive applications. *Optik (Stuttg)*. 2018;165:408-415.
DOI:10.1016/j.ijleo.2018.03.091.
38. Essam Y, El-Nowihy GH. N-Co-Cd-doped TiO₂ nanocomposite for efficient dye-synthesized solar cells. *Ain Shams Eng J*. 2023;102180.
DOI:10.1016/j.asej.2023.102180.
39. Mansour SA, Farha AH, Kotkata MF. Sol-gel synthesized Co-doped anatase TiO₂ nanoparticles: Structural, optical, and magnetic characterization. *J Inorg Organomet Polym Mater*. 2019;29(4):1375-1382.
DOI:10.1007/s10904-019-01102-6.
40. Akpan UG, Hameed BH. Advancements in sol-gel method of doped-TiO₂ photocatalysts. *Appl Catal A Gen*. 2010; 375:1-11.
DOI:10.1016/j.apcata.2009.12.023.
41. Wang Y, Cheng H, Hao Y, Ma J, Li W, Cai S. Photoelectrochemical properties of metal-ion-doped TiO₂ nanocrystalline electrodes.
42. Dhanalekshmi KI, Magesan P, Umopathy MJ, Zhang X, Srinivasan N, Jayamoorthy K. Enhanced photocatalytic and photodynamic activity of chitosan and garlic loaded CdO-TiO₂ hybrid bionanomaterials. *Sci Rep*. 2021;11(1): 20790.
DOI:10.1038/s41598-021-00242-5.
43. Ranjitha A, Muthukumarasamy N, Thambidurai M, Velauthapillai D. Enhanced photovoltaic performance of quantum dot sensitized solar cells with Ag-doped TiO₂ nanocrystalline thin films. *J Mater Sci Mater Electron*. 2014;25(6):2724-2729.
DOI:10.1007/s10854-014-1935-x.
44. Kunnamareddy M, Rajendran R, Sivagnanam M, Rajendran R, Diravidamani B. Nickel and sulfur codoped TiO₂ nanoparticles for efficient visible light photocatalytic activity. *J Inorg Organomet Polym Mater*. 2021;31(6):2615-2626.
DOI:10.1007/s10904-021-01914-5.
45. Douven S, et al. Cost-effective visible LED light: From powders to films.
46. Kiani MN, et al. Synthesis and characterization of cobalt-doped ferrites for biomedical applications. 2023;2-8.
DOI:10.1021/acsomega.2c05226.
47. Naveen N. Investigation on physiochemical properties of Mn substituted spinel cobalt oxide for supercapacitor applications; 2019.
DOI:10.1016/j.electacta.2014.01.161.
48. El Mragui A, Zegaoui O, Daou I, Esteves da Silva JCG. Preparation, characterization, and photocatalytic activity under UV and visible light of Co, Mn, and Ni mono-doped and (P,Mo) and (P,W) co-doped TiO₂ nanoparticles: A comparative study. *Environ Sci Pollut Res*. 2021;28(20):25130-25145.
DOI:10.1007/s11356-019-04754-6.
49. Garg A, et al. Photocatalytic degradation of bisphenol-A using N, Co codoped TiO₂ catalyst under solar light. *Sci Rep*. 2019;9(1):1-13.
DOI:10.1038/s41598-018-38358-w.
50. Pirbazari AE, Monazzam P, Kisomi BF. Co/TiO₂ nanoparticles: Preparation, characterization, and its application for photocatalytic degradation of methylene blue. *Desalin Water Treat*. 2017;63:283-292.
DOI:10.5004/dwt.2017.20205.
51. Aqeel M, et al. TiO₂Co-doped with Zr and Ag shows highly efficient visible light photocatalytic behavior suitable for treatment of polluted water. *RSC Adv*. 2020;10(69):42235-42248.
DOI:10.1039/d0ra08718a.
52. Bahrami S, Ahmadpour A, Rohani Bastami T, Ayati A, Mirzaei S. Comparative study of metal nanoparticles anchored TiO₂ using polyoxometalate intermediate in photodegradation of azo dye pollutant in aquatic environments. *Inorg Chem Commun*. 2024;160:111986.
DOI:10.1016/J.INOCHE.2023.111986.
53. Maučec D, Šuligoj A, Ristić A, Dražić G, Pintar A, Tušar NN. Titania versus zinc oxide nanoparticles on mesoporous silica supports as photocatalysts for removal of dyes from wastewater at neutral pH. *Catal Today*. 2018;310:32-41.
DOI:10.1016/j.cattod.2017.05.061.
54. Lee KH, et al. The comparison of metal doped TiO₂ photocatalytic active fabrics under sunlight for wastewater treatment applications. *Catalysts*. 2023;13(9):1293.
DOI:10.3390/catal13091293.
55. Phuruangrat A, Mad-Ahin S, Yayapao O, Thongtem S, Thongtem T. Photocatalytic degradation of organic dyes by UV light, catalyzed by nanostructured Cd-doped ZnO synthesized by a sonochemical method. *Res Chem Intermed*. 2015;41(12):9757-9772.

- DOI:10.1007/s11164-015-1963-z.
56. Jahdi M, Mishra SB, Nxumalo EN, Mhlanga SD, Mishra AK. Smart pathways for the photocatalytic degradation of sulfamethoxazole drug using F-Pd co-doped TiO₂ nanocomposites. Appl Catal B Environ. 2020;267(October 2019):118716. DOI:10.1016/j.apcatb.2020.118716.

Disclaimer/Publisher's Note: The statements, opinions and data contained in all publications are solely those of the individual author(s) and contributor(s) and not of the publisher and/or the editor(s). This publisher and/or the editor(s) disclaim responsibility for any injury to people or property resulting from any ideas, methods, instructions or products referred to in the content.

© Copyright (2024): Author(s). The licensee is the journal publisher. This is an Open Access article distributed under the terms of the Creative Commons Attribution License (<http://creativecommons.org/licenses/by/4.0>), which permits unrestricted use, distribution, and reproduction in any medium, provided the original work is properly cited.

Peer-review history:

The peer review history for this paper can be accessed here:

<https://www.sdiarticle5.com/review-history/126730>